Journal of the Korean Society of Remote Sensing, Vol. 14, No.4, 1998, pp.366~375

Identifying Yellow Sand from the Ocean Color Sensor SeaWiFS Measurements

Byung-Ju Sohn and Seok-Gyu Hwang

Department of Earth Sciences, Seoul National University

해색 센서 SeaWiFS 관측을 이용한 황사 판독

손병주 · 황석규

서울대학교 지구과학교육과

Abstract

Optical characteristics of the yellow sand and their influences on the ocean color remote sensing has been studied using ocean color sensor SeaWiFS measurements. Two cases of April 18 and April 25, 1998, representing yellow sand and background aerosol, are selected for emphasizing the impact of high aerosol concentration on the ocean color remote sensing. It was shown that NASA's standard atmospheric correction algorithm treats yellow sand area as either too high radiance or cloud area, in which ocean color information is not generated. Optical thickness of yellow sand arrived over the East Asian sea waters in April 18 indicates that there are two groups loaded with relatively homogeneous yellow sand, i.e.: heavy yellow sand area with optical thickness peak around 0.8 and mild area with about 0.4, which are consistent with ground observations. The movement of the yellow sand area obtained from surface weather maps and backward trajectory analysis manifest the notion that the weak yellow sand area was originated from the outer region of the dust storm. It is also noted that high optical thickness associated with the yellow sand is significantly different from what we may observe from background aerosol, which is about 0.2. These characteristics allow us to determine the yellow sand area with an aid of atmospheric correction parameter. Results indicate that the yellow sand area can be determined by applying the features revealed in scattergrams of atmospheric correction parameter and optical thickness.

Received 16 September 1998 ; Accepted 20 December 1998.

요 약

해색 센서인 SeaWiFS의 자료를 이용하여 황사의 광학적 성질과 황사가 해색 원격탐사에 미치는 영향에 대해 연구하였다. 황사가 해색에 미치는 영향을 살펴보기 위해 황사현상이 나타났던 1998년 4월 18일과 맑은 날인 4월 25일의 자료를 선택하였다. NASA 표준 대기 보정 알고리즘은 황사의 영역을 복사휘도가 너무 크거나 또는 구름의 영역으로 간주하여 황사 지역에 대한 해색 정보를 생산하지 않고 있다. 4월 18일 동아시아 해양에 도착한 황사는 에어로졸의 광학적 두께의 관점에서 상대적으로 균질한 두 부류로 구성되어 있음을 보여주었다. 즉, 에어로졸 광학적 두께가 0.8 부근에 최대의 값을 갖는 강한 황사와 0.4 부근의 값을 갖는 약한 황사가 존재하였으며, 이 값들은 지상의 관측 결과와 잘 일치하였다. 지상 일기도의 분석과 경로 역추적을 통해 얻은 황사의 이동은 약한 황사 영역이 먼지 폭풍의 가장자리로부터 기원하고 있음을 암시한다. 또한, 황사와 관련된 에어로졸 광학적 두께가 큰 영역은 약 0.2 정도의 광학적 두께를 갖는 배경 에어로졸과 매우 다름을 알 수 있다. 이러한 에어로졸의 광학적 특성은 대기 보정 변수의 도입과 더불어 황사의 영역을 정량적으로 결정할 수 있음을 가능케 하고 있다. 본 논문의 결과는 대기 보정 변수와 광학적 두께의 분산 그래프에 나타나는 특징을 통해 황사 영역을 결정할 수 있음을 보여준다.

1. Introduction

Aerosols can give significant impact on the global climate either directly, by reflecting more solar energy to the space, or indirectly, by providing cloud condensation nuclei that lead to cloud formation (Hobbs, 1993). Therefore understanding the optical characteristics and their parameterizations are very important to understand the current global climate and environmental changes.

For the past twenty years, geographical origination and temporal variability of the yellow sand have been studied using various field measurements, meteorological analysis, and satellite observations (Uematsu et al., 1983, Nakajima et al., 1989 among many others). In particular, satellite has been useful tool recognizing the extent of yellow sand area. Although satellite remote sensing of aerosol optical characteristics is important for studying direct and indirect impact on the global climate and cloud formation, its use has been limited because of the uncertainties from the lack of sensor capability. Recent development of atmospheric correction algorithms for the ocean color sensors (Gordon and Wang, 1994) such as Nimbus 7 Coastal Zone Color Scanner (CZCS), and Sea-viewing Wide-Field-of-view Sensor (SeaWiFS) provides ample opportunities for scientific investigation and application for examining our environmental changes related to aerosol. That is because those sensors have several sensitive channels in the visible spectral region and one or two channels for only sensing the aerosol effect on the satellite measurements.

In this paper, we examine the optical characteristics of the yellow sand using the SeaWiFS data over the East Asian sea water in the spring of 1998. We also show the impact of the yellow sand dust on ocean color remote sensing by presenting that the current NASA's standard atmospheric correction algorithm produces less reliable ocean color when it is applied for heavy dust events occurred, in particular, during the spring time.

2. Data Set and Analysis

The SeaWiFS is an ocean color sensor launched in 1997. It consists of eight spectral bands; 412, 443, 490, 510, 555, 670, 765, and 865 nm. The last two near-infrared channels are used for determining atmospheric aerosol and thus for atmospheric correction. Nominal spatial resolution is about 1 km at the nadir view. Detailed sensor characteristics are found in Gregg et al. (1994). In this research, we use the reduced resolution global area coverage (GAC) data from the high resolution local area coverage (LAC) data generated by the scanner.

Aerosol optical thickness is obtained from SeaWiFS data by employing the NASA-developed SeaWiFS data processing software, SeaDAS (SeaWiFS Data Analysis System). The atmospheric correction algorithm used in the SeaDAS has two different aspects from CZCS algorithm, i.e.: to consider multiple scattering and to employ aerosol models.

SeaWiFS algorithm utilizes specific aerosol models depending on relative humidity. To describe the SeaWiFS atmospheric correction algorithm, we first begin with the definition of reflectanc ρ :

$$\rho(\lambda) = \pi L(\lambda)/F_0(\lambda)\cos\theta_0 \quad \cdots\cdots (1)$$

where L is upward radiance in the given viewing angle, F_0 is extraterrestrial solar irradiance, and θ_0 is solar zenith angle. Total reflectance (ρ_t) measured at the top of the atmosphere can be expressed by:

$$\rho_t(\lambda) = \rho_r(\lambda)+\rho_a(\lambda)+\rho_{ra}(\lambda)+t\rho_w \quad \cdots\cdots (2)$$

where ρ_r, ρ_a, and ρ_{ra} are reflectances from Rayleigh scattering, Mie scattering associated with loaded aerosols, and from interactions between air molecules and aerosols. And ρ_w is water-leaving reflectance that can be used for determining in-water content such as pigment concentration.

The definition of diffuse transmittance t is as follows:

$$t = \exp[\tau_r/2+\tau_{oz})/\cos\theta] \quad \cdots\cdots (3)$$

where τ_r, τ_{oz} are optical thickness due to Rayleigh scattering and ozone absorption. And θ is satellite zenith angle.

For the calculation of aerosol influence on the total reflectance, SeaWiFS algorithm employs 12 aerosol models, i.e.: oceanic models with relative humidity 90 and 99% of relative humidity, maritime models with 50, 70, 90 and 99%, coastal and tropospheric models with 50, 90 and 99% of relative humidity.

Since there is a near-linear relationship between aerosol multiple scattering and single scattering, it is possible to calculate multiple scattering ($\rho_a+\rho_{ra}$) using single scattering effect (ρ_{as}) with an aid of near-linear relationship between them (Gordon and Wang, 1994). Because water-leaving radiance is nearly zero for SeaWiFS band 7 (765 nm) and band 8 (865 nm), it is logical to use these bands to assess the aerosol properties and deduce aerosol effects in other bands. To determine two aerosol models, atmospheric correction parameter $\varepsilon(765,865)$ is used.

$$\varepsilon(\lambda_i, \lambda_j) = \frac{\rho_{as}(\lambda_i)}{\rho_{as}(\lambda_j)} = \frac{\omega_a(\lambda_j)\tau_a(\lambda_j)P_a(\theta, \theta_0, \lambda_i)}{\omega_a(\lambda_j)\tau_a(\lambda_j)P_a(\theta, \theta_0, \lambda_j)} \quad \cdots\cdots (4)$$

where, ω_a is single scattering albedo and P_a is aerosol scattering phase function.

Because water leaving radiance in near IR region (765 and 865 nm for SeaWiFS channels) is nearly zero, we can compute aerosol effect by removing Rayleigh scattering, ozone absorption, and multiple scattering from the total reflectance, as in Eq. (2). Rayleigh scattering and ozone absorption are relatively easy to compute, and thus the problem of calculating water leaving radiance comes down to how we calculate aerosol influences. SeaWiFS algorithm calculates the average of $\varepsilon(765,865)$ from 12 aerosol models and selects two aerosol models having nearest $\varepsilon(765,865)$. Assuming aerosol effect at any given location can be expressed by these two aerosol models, we can calculate aerosol single scattering effect and thus multiple scattering effect by applying the same ratio between two selected aerosol models to shorter wavelength.

3. Results

Analyses were performed on two cases of April 18 and 25, selected for contrasting the signal of yellow sand aerosol to the background aerosol. Figs. 1(a) and (b) are SeaWiFS images for April 18 and 25, 1998 respectively. Examining the spatial scale and pattern of the imagery, there is a

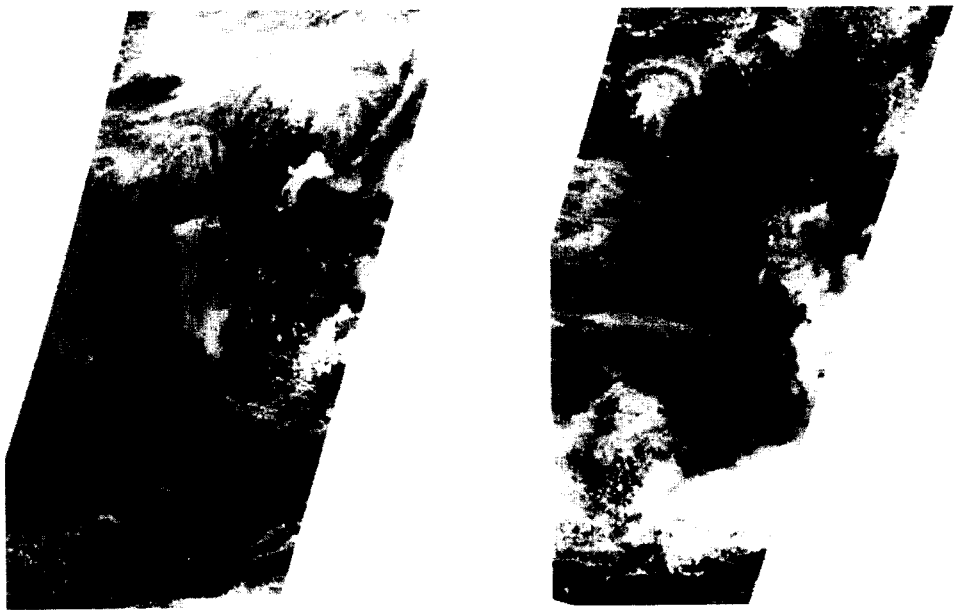

(a) April 18, 1998 (b) April 25, 1998

Fig. 1. Combined images of SeaWiFS channel 1, 5, 6 measurements for (a) April 18, and (b) April 25, 1998.

clear indication of yellow sand aerosol spread over the East China Sea and across the Korean peninsula on April 18. By contrast, mostly dark oceanic area in Fig. 2(b) suggests that it is clear on April 25 and thus it represents a type of background aerosol.

Observations of visibility at surface weather station also clearly indicate that the gray patch of visible image shown in Fig. 1(a) over the East China Sea is associated the yellow sand (Fig. 2a). The yellow sand area located over the North China and Mongolia on April 15 moved to Central China on April 16. And it further moved to the East China Sea in following two days. Therefore gray-patched area in Fig. 1(a) over the East China Sea is coincident with yellow sand area inferred from surface weather maps. We analyzed backward trajectories of three air masses given in Fig. 2(b). For the computation of trajectory we use ECMWF analysis of meteorological parameters. Fig. 2(b) shows the trajectories on 300K isentropic surface (potential temperature). Most southwestern path is very consistent with that suggested in the surface observations of visibility. Getting away from the center of the gray-patched area over the East China Sea shown in Fig. 1(a), the air mass is originated from the eastern part of Mongolia.

Fig. 3(a)-(b) are the calculated aerosol optical thickness at 765 nm for April 18 and 25, respectively. Considering April 25 is not related to the yellow sand, the aerosol optical thickness of

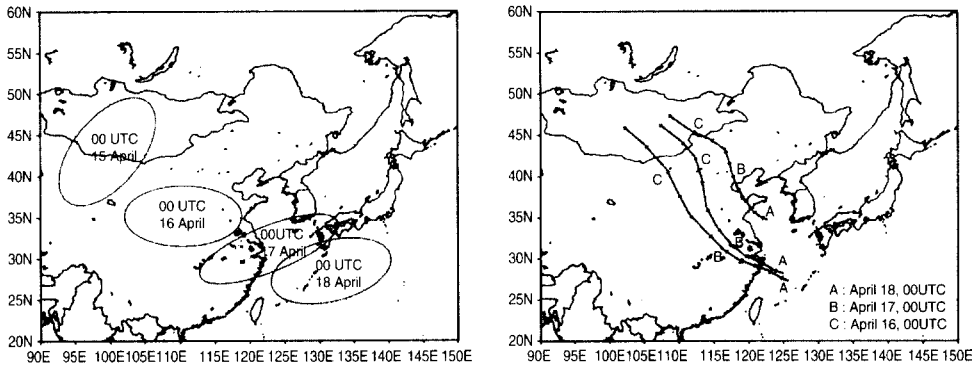

(a) (b)

Fig. 2. The movement of yellow sand area occurred in April 15, 1998 over inner Mongolia (a), and backward trajectories from three locations of yellow sand area in the East Asian sea water inferred from the SeaWiFS image (b).

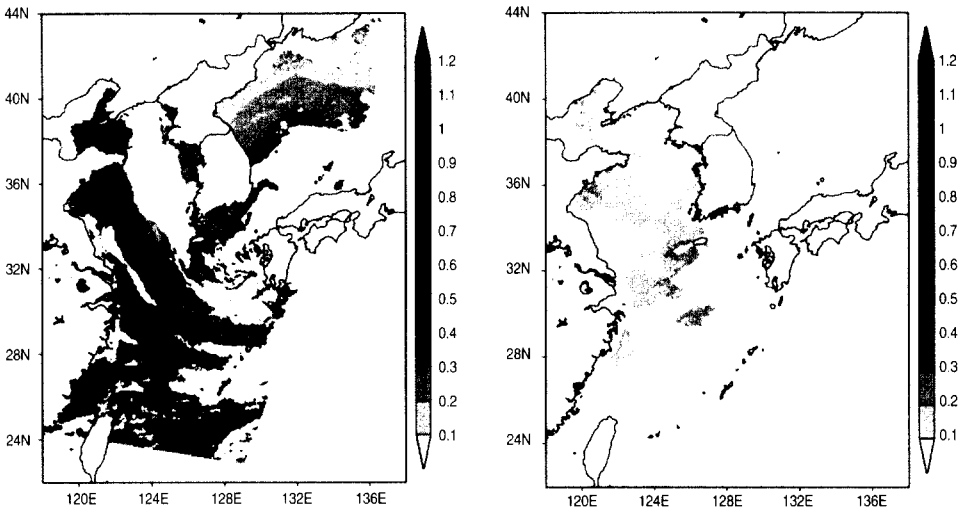

(a) April 18, 1998 (b) April 25, 1998

Fig. 3. Aerosol optical thickness at 765 nm for (a) 18 April 1998, and (b) 25 April 1998.

0.2-0.3 may represent characteristics of the typical tropospheric aerosol over East Asia. By contrast, aerosol optical thickness for April 18 shows that optical thickness of the yellow sand is ranging from 0.6 to 1.0. These values are in good agreement with results obtained from ground observations of direct solar radiation. We measured direct and diffuse solar radiation at the

background atmosphere monitoring site (36.517°N, 126.317°E) in Anmyon Do which is located on the west coast of the Korean peninsula. Detailed descriptions of these measurements and results are found by Sohn et al. (1998). Thus, the SeaWiFS atmospheric correction algorithm resolves the features of yellow sand dust even though the yellow sand is not included as a class of aerosol in the SeaWiFS atmospheric correction algorithm. In other words, the NASA's algorithm in SeaDAS seems to be useful even for the computation of optical thickness of yellow sand aerosol.

The characteristics of aerosol optical thickness are more evident in the histogram of percentage area with an optical thickness presented in Fig. 4. The optical thickness for April 18 obtained from the original algorithm (without changing the albedo criteria used for screening cloud scene) shows around 0.2 which is consistent with the values for April 25. However, aerosol optical thickness obtained by enhancing the criteria of albedo to 2.6% as a cloud threshold results in three peaks; 0.23, 0.4, and 0.8. The value around 0.8 covers most of yellow sand area. Surrounding the yellow sand area is the second largest peak of aerosol optical thickness. From the trajectory analysis of Fig. 2 this area is corresponding to the east side of the main dust storm area in Mongolia, thus it is likely weaker dust storm area in which aerosol optical thickness is somewhat weaker than the center of the storm. Therefore, the yellow sand area in Fig. 3 includes two parts; an area showing optical thickness around 0.8 and the surrounding area with aerosol optical thickness around 0.4. Similar values are found in the retrieved aerosol optical thickness from the ground-based solar radiation measurements for April 28 in which a weak yellow sand event occurred. Based on the trajectory analysis and ground-based optical thickness measurement, two peaks around 0.4 and 0.8 of optical thickness are related to the yellow sand.

Fig. 5 shows scattergram of the aerosol optical thickness at 765 nm and the atmospheric

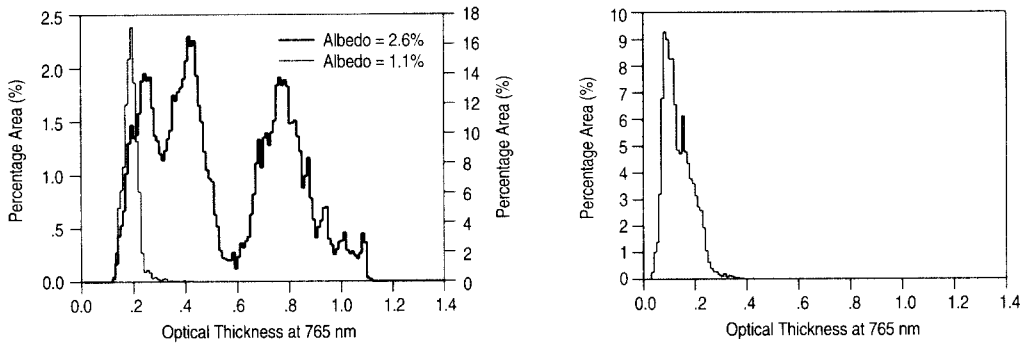

(a) April 18, 1998 (b) April 25, 1998

Fig. 4. Distributions of percentage area of aerosol optical thickness at 765 nm for (a) 18 April 1998, and (b) 25 April 1998. Note changed scale in the right ordinate of (a) for the original setting for the cloud threshold.

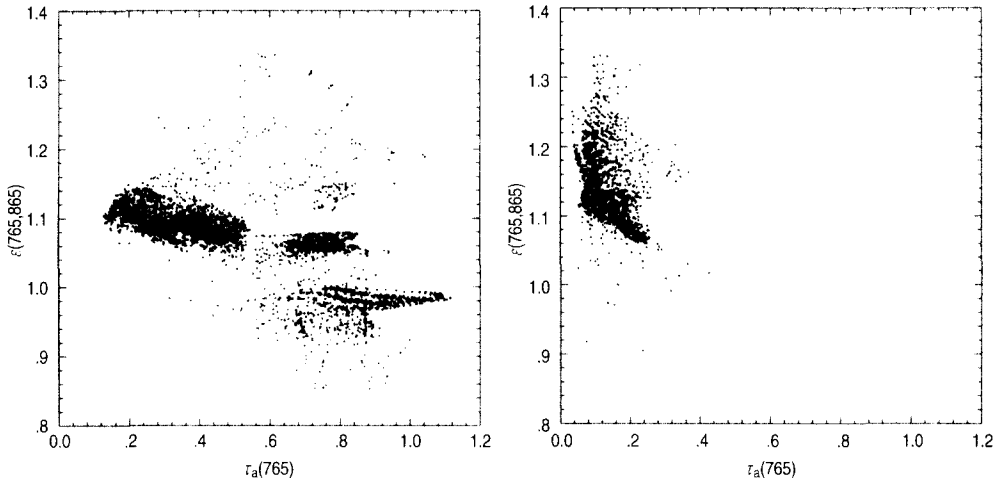

(a) April 18, 1998 (b) April 25, 1998

Fig. 5. Scattergram of atmospheric correction parameter (ε) and aerosol optical thickness (τ_a) for (a) April 18, 1998, and (b) April 25, 1998.

correction parameter ε between 765 nm and 865 nm for April 18 and April 25. Striking difference is found in the features of scattering. In April 18, main values of ε are found between 1.05 and 1.15 widely varying with optical thickness from 0.2 and 0.85. The ε values smaller than 1.0 are considered to be cloud-contaminated pixels since they are mostly located in the cloud edge area. On the other hand, the ε distributions in April 25 shows wider variation of ε while optical thickness is much smaller and is confined around 0.2, comparing to the yellow sand case of April 18. This significantly different pattern of ε suggest that the yellow sand areas can be determined from SeaWiFS data by applying features obtained from atmospheric correction parameter and optical thickness.

Even though the optical thickness retrieved from SeaWiFS data is in good agreement with ground-observed values, distributions of CZCS type pigment concentration for April 18 shows erroneous results, compared to those of the background aerosol case measured seven days later (April 25) – see Fig. 6. For example, pigment concentration around 10 μg/liter is found over the yellow sand area between Yangtze basin and Cheju island whereas 3-4 μg/liter of the concentration is noted in the same area seven days later. These differences suggest a new scheme resolving the influence of yellow sand for processing the Asian dust-laden SeaWiFS scene. The inclusion of the Asian dust in the OCTS algorithm develpoed by Fukushima et al. (1997) may also help SeaWiFS data produce more realistic results even in the case of yellow sand event.

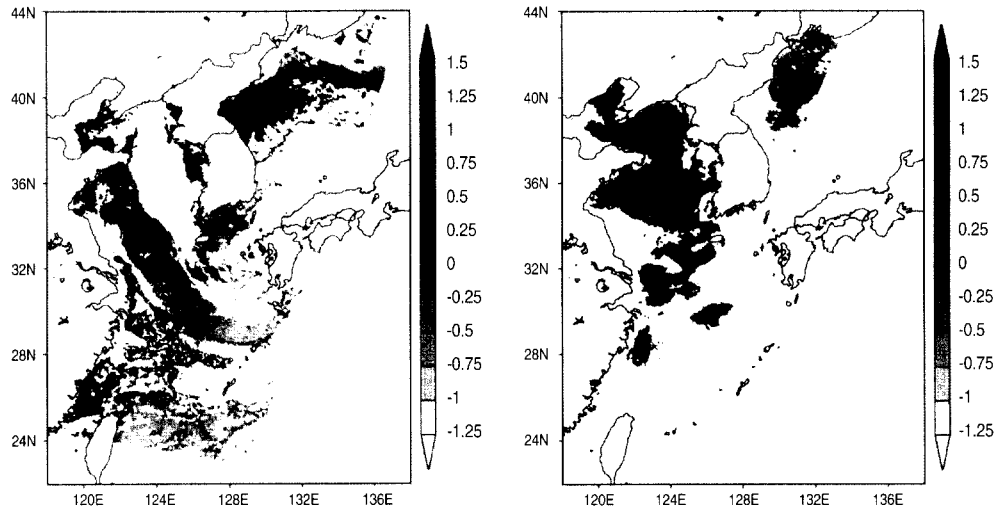

(a) April 18, 1998 (b) April 25, 1998

Fig. 6. CZCS type pigment concentrations obtained by applying SeaWiFS atmospheric correction algorithm for (a) 18 April 1998, and (b) 25 April 1998.

4. Summary and Conclusions

A dust storm occurred over inner Mongolia in April 15, 1998 and its associated yellow sand aerosol moved over the East China Sea and the Yellow Sea by April 18, 1998. Optical parameters of the yellow sand noticed in April 18, 1998 were retrieved from the SeaWiFS ocean color sensor measurements. Also obtained are optical parameters for April 25, 1998, contrasting the yellow sand aerosol with clear-sky background aerosol. In this process, we employed SeaDAS software which uses atmospheric correction algorithm developed by Gordon and Wang (1994).

It was noted that the optical thickness of yellow sand aerosol is around 0.8, far higher than the typical aerosol optical thickness of 0.2 for the clear sky of April 25. This value is consistent with the result obtained from ground-based solar radiation measurements. Also noted is the relatively smaller aerosol optical thickness (around 0.4) over the marginal yellow sand area, comparing with the center of the yellow sand area. Considering that this value is larger than 0.2 for the clear sky and it is originated from the outer side of the dust storm area, we suspect that it is the weak yellow sand area.

Taken optical parameters together we showed a way that can lead to quantitatively identify the extent of yellow sand area from the SeaWiFS measurements. Distinct differences between the yellow sand and background case are clearly shown in the scattergram of the atmospheric

correction parameter (ε) versus aerosol optical thickness. Based on these fidndings we conclude that it is possible to identify the yellow sand area using SeaWiFS measurements. However, the obtained CZCS type pigment concentrations over the yellow sand area indicate that the SeaWiFS atmospheric correction algorithm need to be improved, in particular, for the area covered with yellow sand. Inclusion of specific yellow sand model into the algorithm may be necessary.

Acknowledgments

Authors express their gratitude to Profs. T. Nakajima, H. Fukushima, and Dr. A. Higurashi for valuable discussions and suggestions. This research was performed under the project 'Cal/Val and Marine Application of OSMI' (97-NR01-02-A) supported by Ministry of Science and Technology of Korea.

References

Gregg, W.W., F.S. Patt, R.H. Woodward, 1994: The simulated SeaWiFS data set, Version 2. *NASA Technical Memorandum* 104566, Vol. 15, 42pp.

Fukushima, H., T. Noguchi, H, Tabata, and M. Toratani, 1997: Evaluation of OCTS atmospheric correction and possible improvement. *Proceeding of International Symposium on Remote Sensing*, Korean Society of Remote Sensing and EMSEA, Nov. 5-7, 1997, Pusan, 262-268.

Gordon, H. R., and M. Wang, 1994: Retrieval of water-leaving radiance and aerosol optical thickness over the oceans with SeaWiFS : A preliminary algorithm, *App. Opt.*, 33, 443-452.

Hobbs, P.V., 1993: Aerosol-cloud-climate interactions. Edited by P.V. Hobbs, Academic Press, 233pp.

Nakajima, T., M. Tanaka, M. Yamano, M. Shiobara, K. Arao, and Y. Nakanishi, 1989: Aerosol optical characteristics in the Yellow Sand events observed in May, 1982 at Nagasaki. Part II. Model. *J. Meteor. Soc. Japan*, 67, 279-291.

Sohn, B.J., D.S. Shin, and S.S. Lee, 1998: Optical Characteristics of Yellow Sand from Ground-Based Solar Radiation Measurements near the Yellow Sea. *Proceeding of International Symposium on Remote Sensing*, Korean Society of Remote Sensing and EMSEA, Sep. 16-18, 1998, Kwangju ,9-13.

Uematsu, M., R. Duce, J.M. Prospero, L. Chen, and J.T. Merrill, and R.L. McDonald, 1983: Transport of mineral aerosol from Asia over the North Pacific ocean. *J. Geophys. Res.*, 88, 5343-5352.